Direct observation of potential profiles with a 200 keV heavy ion beam probe on the Compact Helical System

A. Fujisawa, H. Iguchi, S. Lee, T. P. Crowley,[a] Y. Hamada, S. Kubo, H. Idei, H. Sanuki, K. Itoh, T. Minami, K. Tanaka, S. Nishimura, K. Ida, S. Hidekuma, M. Kojima, C. Takahashi, S. Okamura, and K. Matsuoka
National Institute for Fusion Science, Furo-cho, Chikusa-ku, Nagoya, 464-01, Japan

(Received 31 October 1996; accepted 7 February 1997)

In this paper we present space potential profiles directly observed in a toroidal helical plasma of the Compact Helical System (CHS) [K. Matsuoka *et al.*, *Proceedings, 12th International Conference on Plasma Physics and Controlled Nuclear Fusion*, Nice, 1988 (International Atomic Energy Agency, Vienna, 1989), Vol. 2, p. 411], using a 200 keV heavy ion beam probe. The potential profiles exhibit widely varied characteristics, including positive and negative polarities for electron cyclotron and neutral beam-heated plasmas, respectively. The behavior of high-energy particles in the CHS plasmas are deduced from loss cone diagrams evaluated from the observed potential profiles. [S1070-664X(97)02505-6]

I. INTRODUCTION

Intrinsic rotational transform of the vacuum magnetic field is an advantage of toroidal helical plasmas for realization of a steady-state fusion reactor. However, helical ripples of the magnetic field structure give birth to a large deviation of high-energy particle orbits from the magnetic flux surfaces,[1] which results in deterioration of confinement and heating efficiency in the collisionless regime. The problem is more severe in a device of small aspect ratio because of its larger loss cone region, although it is superior from an economical point of view.[2] The plasma potential is a key physics quantity affecting the loss cone structure by giving $E\times B$ rotation to helically trapped particles.

Even in tokamaks, discoveries of the high confinement mode (H mode)[3] and other improved confinement modes have stimulated interest in radial electric fields and potential structures associated with the mode transitions.[4] Potential profiles were measured in the Impurity Study Experiment-B(ISX-B) tokamak and the Texas Experimental Tokamak (TEXT) with heavy ion beam probes (HIBP).[5,6] However, the complicated beam trajectories in toroidal helical devices prevented from the easy application of an HIBP to measure potential profiles. Direct measurements of accurate potential profile are, however, significantly important in a toroidal helical device to investigate loss cone structure and effects of electric field shear on the confinement properties.

The first application of HIBP measurements in a toroidal helical plasma, using a traditional method,[7] was performed on electron cyclotron heated (ECH) plasmas of the Advanced Toroidal Facility (ATF). In the Compact Helical System (CHS),[8] which is a heliotron/torsatron device with a low aspect ratio (~ 5), the radial electric field was originally deduced from impurity rotation velocity using charge exchange recombination spectroscopy (CXS).[9,10] Recently, a 200 keV HIBP was constructed to more directly measure the potential in CHS. The HIBP uses a new idea to manage complicated probing beam trajectories, which is *termed active trajectory control*.[11,12] With this method, we have succeeded in measuring radial profiles of electrostatic potentials (or electric fields) in the CHS plasmas, covering all plasma radii within a short period (a few ms) of a discharge. In this paper, we will present potential profiles of ECH and neutral beam injection (NBI) heated plasmas in a low-density regime, and will discuss the relationship between loss cone structure and potential, and their roles on heating efficiency and confinement of high-energy particles.

II. EXPERIMENTAL SETUP

CHS is a heliotron/torsatron device whose major radius is $R_0 = 1.0$ m, and averaged minor radius is $\overline{a} = 0.2$ m; hence the aspect ratio is $R/\overline{a} = 5$. CHS has a pair of helical winding coils and four pairs of poloidal coils to control the position and shape of the plasma. The magnetic field configuration has a periodicity of $l = 2$ and $m = 8$ in poloidal and toroidal directions, respectively. The potential measurements here were performed in the magnetic configuration, whose axis was located at $R_{ax} = 0.921$ m, and with a field strength of 0.9 T. In the present experiments, a hydrogen neutral beam system or a 53 GHz gyrotron were used to sustain the hydrogen plasma.

In potential measurements with HIBPs, singly charged heavy ions (primary beam) are injected into a target plasma, and then doubly charged ions are created by an electron impact ionization (secondary beam). They come out with an energy change corresponding to plasma potential at the ionization point. In the case of toroidal helical devices, the secondary beams coming from different observation points are widely distributed in entrance positions and angles at the energy analyzer. This problem causes restrictions in the observation range and energy measurement errors due to an uncertainty in the beam injection angle. A unique feature of CHS HIBP is that the beam trajectories are controlled using a secondary beam sweep system, in addition to the standard primary beam system. This beam control method is based on

[a]Also at the Rensselaer Polytechnic Institute, Troy, New York 12181.

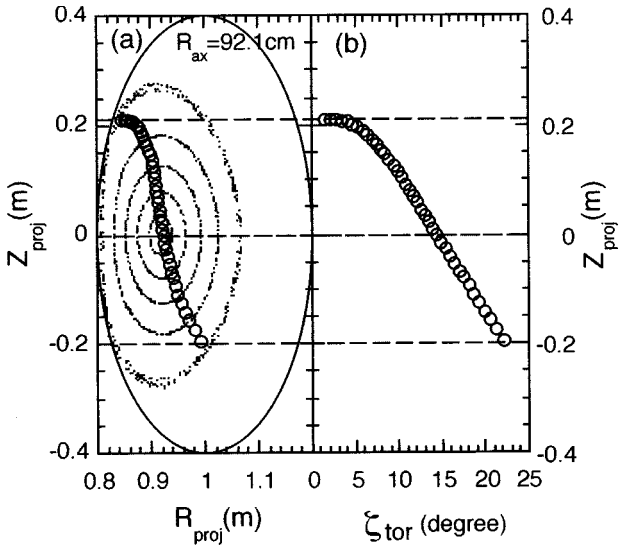

FIG. 1. (a) Observation points projected onto a vertically elongated cross section of magnetic flux surfaces for the case of a magnetic field configuration with the axis location of 92.1 cm. (b) Toroidal angle of the actual observation points. The angle is measured from the vertically elongated cross section.

a guiding principle[11] to determine sweep voltages and observation points, and gives the following advantages to the CHS HIBP: (1) a wider observation range, (2) reduction in the energy measurement errors, and (3) allowance for the energy analyzer location at a sufficient distance from the plasma to avoid uv loading and a leakage magnetic field.

The observation points are illustrated in Fig. 1(a), when a 72 keV cesium beam is used for the magnetic field configuration, where the experiments were performed. The points in the figure are the projections obtained by tracing magnetic field lines from the actual observation points. The toroidal angles of the observation points are also shown in Fig. 1(b), where $\zeta=0°$ is the toroidal position of a vertically elongated flux surface. The points are distributed along the toroidal direction over about half of the helical pitch (45°). In gas ionization experiments, it was confirmed that the sweep voltage combinations for these observation points lead secondary beams into the energy analyzer at the proper angles and positions. The error caused by uncertainty in the beam injection angle into the analyzer is estimated to be less than 10 V.[12]

III. POTENTIAL PROFILES

Figure 2(a) shows potential profiles obtained during steady-state ECH and NBI plasmas. The open and closed circles indicate the potential profiles of ECH plasmas with low ($\overline{n_e}=3\times10^{12}$ cm^{-3}) and medium density ($\overline{n_e}=8\times10^{12}$ cm^{-3}), respectively. The central electron temperatures of the low and medium density cases are $T_e(0)=900$ eV and $T_e(0)=400$ eV, respectively. The squares indicate the potential profile of a coinjected NBI plasma where the line-averaged electron density is $\overline{n_e}=8\times10^{12}$ cm^{-3}, and the electron and ion temperatures

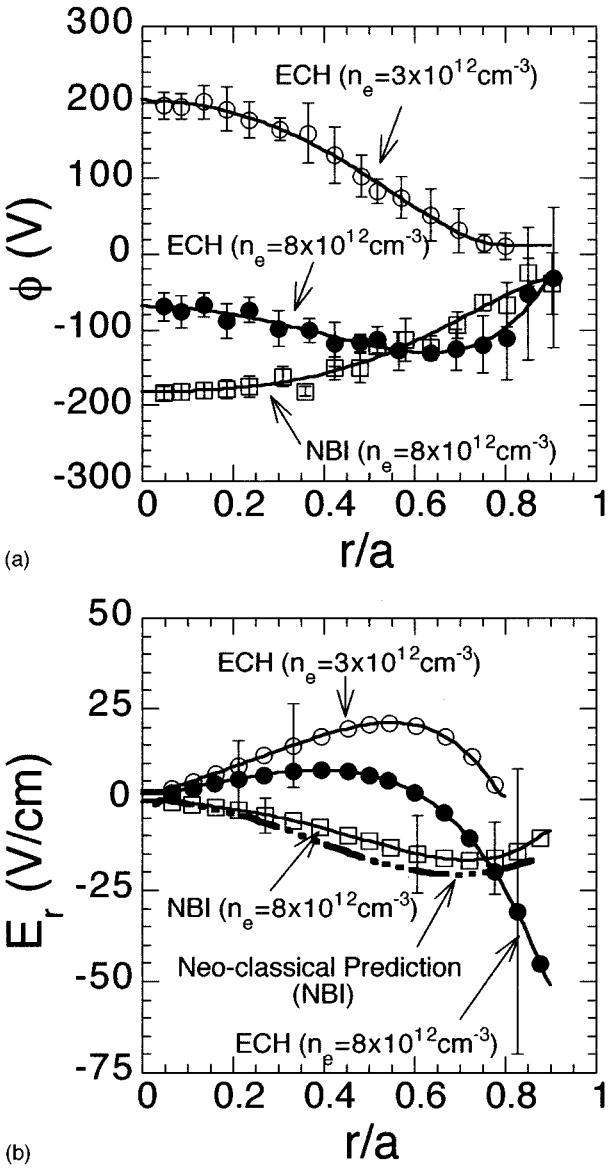

FIG. 2. (a) Potential profiles measured with a 200 keV HIBP. The open and closed circles represent potential profiles of low ($\overline{n_e}=3\times10^{12}$ cm^{-3}) and medium-density ($\overline{n_e}=8\times10^{12}$ cm^{-3}) ECH plasmas, respectively. The squares are the potential profile of a low-density tangentially coinjected NBI plasma ($\overline{n_e}=8\times10^{12}$ cm^{-3}). (b) Radial electric field profiles deduced from the potential profiles. The dot–dashed line represents a radial electric field predicted from a theory for the low-density NBI-heated plasma case.

are $T_e(0)=300$ eV and $T_i(0)=200$ eV, respectively. These profiles are averages of steady states for about 20 ms, and the error bars are mean standard deviations.

The potential is positive with a central value of about 200 V for a low-density ECH plasma, where the electrons are nearly collisionless since the electron collisionality is $\nu_e^*(\overline{a/2})=1.4$. The definition of the collisionality here is $\nu^*(r)=\nu_{\rm eff}(r)/\omega_b(r)$, with $\nu_{\rm eff}=\nu/\epsilon_h$ and $\omega_b=\iota(\epsilon_h T/m)^{1/2}/2\pi R$, where ι, ν, and ϵ_h are the rotational transform, the collision frequency, and the helical ripple coefficient, respectively. In the medium-density ECH plasma, the potential profile exhibits an interesting characteristic: the electric field is positive in the core, while it has a large negative value ($\simeq$70 V/cm) near the edge. The electron collision-

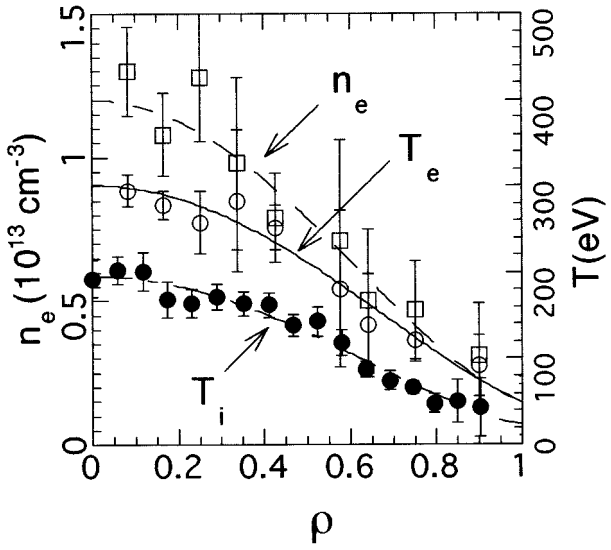

FIG. 3. Plasma parameters in the NBI plasma. The open and closed circles show electron and ion temperatures, respectively. The squares indicate the electron density.

ality is $\nu_e^*(\overline{a/2})=13.1$, and the electrons are in the plateau regime. On the other hand, the potential in the NBI plasma is negative, with a central value of about -200 V. The collisionalities of electrons and ions are $\nu_e^*(\overline{a/2})=6.0$ and $\nu_i^*(\overline{a/2})=8.2$, respectively. The electrons and ions are both in the plateau regime.

Figure 2(b) shows radial electric field profiles deduced from polynomial fits to the measured potential profiles. In the ECH plasmas, there is a tendency for the positive electric field to turn more negative as the density increases. In the medium-density case, the electric field shows a strong shear near the plasma edge although the statistical error bar is large. In the NBI case, ion temperature, electron density, and electron temperature profiles are available from the database. Hence, the experimentally obtained electric field can be compared with the electric-field predicted by the ambipolarity condition $\Gamma_i^{\mathrm{NC}}(E_r)=\Gamma_e^{\mathrm{NC}}(E_r)$, where $\Gamma_i^{\mathrm{NC}}(E_r)$ and $\Gamma_e^{\mathrm{NC}}(E_r)$ represent the electron and ion fluxes in neoclassical theory.[13–15] The dash–dotted line in Fig. 2(b) shows this neoclassical radial electric field. The plasma parameters used in the neoclassical calculation are shown in Fig. 3. The theoretically expected electric field is very similar to the experimental one.

IV. LOSS CONE DIAGRAMS

In toroidal plasmas, the important role of the radial electric field on confinement (e.g., through absolute trapping of particles, suppression of turbulence, or heating efficiency) has been discussed. Particularly, in toroidal helical plasmas, the radial electric field has a significant effect on helically trapped particle orbits whose guiding center motion is expressed by $d\theta/dt=V_\perp\cos\theta/r+\omega_{E\times B}+\omega_{\nabla B}$, where θ, $V_\perp$, $\omega_{E\times B}$, and $\omega_{\nabla B}$ represent the poloidal angle, the toroidal drift velocity, and the rotational angular velocities due to the $E\times B$ and ∇B drifts. Here, the definitions are $V_\perp=\epsilon_t W/qBr$, $\omega_{E\times B}=E/Br$, $\omega_{\nabla B}=\epsilon_h W/qBr^2$, with W and q being the energy and the charge, respectively. If the resonance condition $\omega_{E\times B}+\omega_{\nabla B}\simeq 0$ (or $W\simeq -q\phi/\epsilon_h$) is satisfied, the helically trapped particles escape from the plasma due to their toroidal drift, resulting in a larger loss cone.

An analytical formula can be used to evaluate loss cone boundaries for electrons and ions, when the potential profile is a monotonically decreasing or increasing function.[13,16] The loss cone boundaries for deeply trapped particles are expressed as $W_m<W<W_p$, where W is the particle energy, $W_m=-q\phi(0)f(x)/[\epsilon_{ha}(1-x^2)+\epsilon_{ta}(1-x)]$, and $W_p=-q\phi(0)f(x)/[\epsilon_{ha}(1-x^2)-\epsilon_{ta}(1+x)]$. Here, ϵ_{ta} and ϵ_{ha} represent the toroidal and helical ripple coefficients, x indicates the horizontal coordinate whose origin is on the magnetic axis, and $f(x)$ is a normalized function fitted to the experimental profiles with $f(0)=1$ and $f(\pm 1)=0$. The loss cone for deeply trapped ions of the NBI plasma was evaluated using the observed potential profile, as is shown in Fig. 4(a). The values of $\epsilon_{ta}=0.16$ and $\epsilon_{ha}=0.255$ have been assumed. The loss cone plays a role when the helically trapped particles can complete one poloidal orbit without a collision. This criterion is roughly expressed as $\omega_{\nabla B}>\nu/\epsilon_h$. Figure 4(a) plots the energy W_{rot} needed to satisfy this criterion, which is explicitly written as $W_{\mathrm{rot}}^{2.5}(\mathrm{eV})>1.4\times 10^{-2}n_e(\mathrm{cm}^{-3})B(\mathrm{T})r(\mathrm{cm})^2\epsilon_h^{-2}$. This criterion is not valid near the magnetic axis because the banana width is larger than the local structure due to the small poloidal field.

The neutral beam is tangentially injected into CHS plasmas with an energy of about 35 keV [the hatched region in Fig. 4(a)]. The energy transfer rate from the high-energy beam particles to the bulk ions and electrons is a function of electron temperature. The beam energy that heats ions and electrons equally is given by $W_{pi=pe}=15T_eA_b(Z_i^2/A_i)^{2/3}$, where A_b, A_i, and Z_i are the atomic mass of the beam particles and the atomic mass and the charge of the bulk plasma particles, respectively. Above this energy ($\sim 15T_e$), the beam particles selectively heat electrons, preserving pitch angle. Below this energy, the injected beam particles experience pitch angle scattering, and simultaneously transfer their energy to the bulk ions. It becomes, therefore, more probable for the beam particles to enter the loss cone below this energy.

In CHS, effective energy transfer from the injected beams to the bulk ions occurs in the regime between the upper loss cone boundary and $W_{pi=pe}(=15T_e)$. The bulk ion temperature is below the lower loss cone boundary. Hence, the bulk ions are confined by $E\times B$ rotation. If the potential becomes sufficiently negative so that the loss cone region is located above $W_{pi=pe}$, then the ion heating efficiency will be improved since pitch angle scattering only occurs below the loss cone region.

A loss cone diagram for deeply trapped electrons has also been calculated for the low-density ECH plasma with a positive potential. It is shown in Fig. 4(b) that the loss cone region above the energy of W_{rot} exists only on the weak field side ($x>0$). The critical energy W_{rot} for electrons is higher than for ions since the collision frequency is larger for the same energy; $W_{\mathrm{rot}}^{2.5}(\mathrm{eV})>6.3\times 10^{-1}n_e(\mathrm{cm}^{-3})\ B(\mathrm{T})r(\mathrm{cm})^2\epsilon_h^{-2}$. Thus, an electron heated up on the weak field side of the torus will easily enter the loss cone. With this

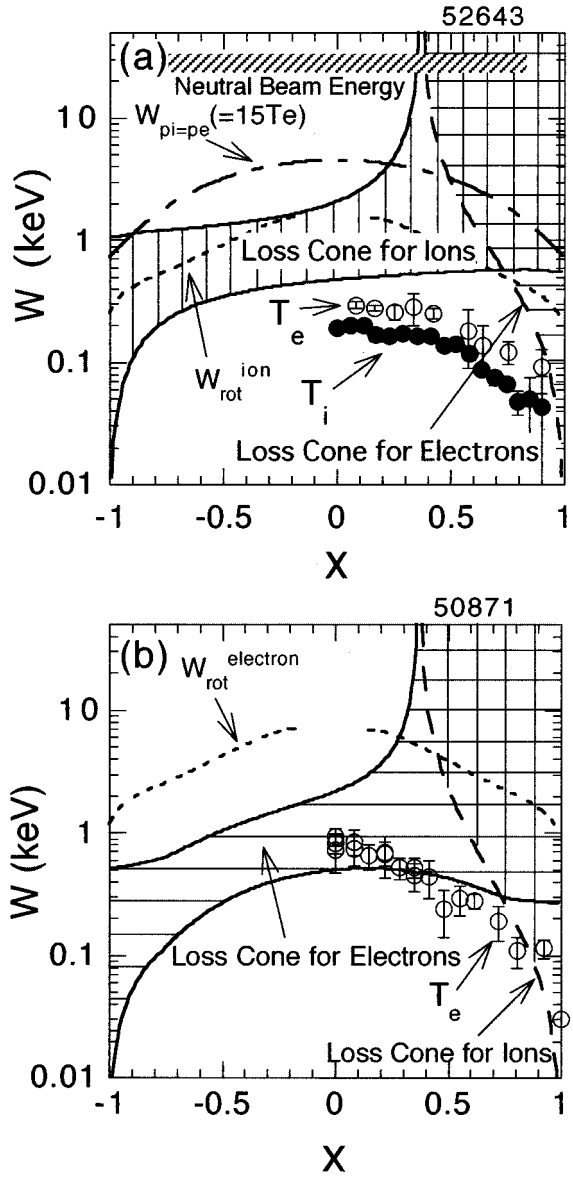

FIG. 4. The loss cone diagrams for deeply trapped particles evaluated from the measured potential profile with the HIBP. The loss cone plays a role in the region above the dashed line $W_{\rm rot}$. This line delineates the (ion or electron) energy at which the particle can complete one poloidal orbit. (a) The ion loss cone for low-density NBI-heated plasma with $\phi(0) = -200$ V. The electron loss cone boundary is also indicated by a dashed line. Along the dot–dashed line $W_{pi=pe}$, energy transfer from the heating beam ions to the bulk electrons and ions occurs equally. The open and closed circles are the electron temperature measured with a Thomson scattering system and the ion temperature measured with a CXR system, respectively. (b) The electron loss cone for low-density ECH plasma with $\phi(0) = 200$ V. The ion loss cone boundary is also indicated by a dashed line.

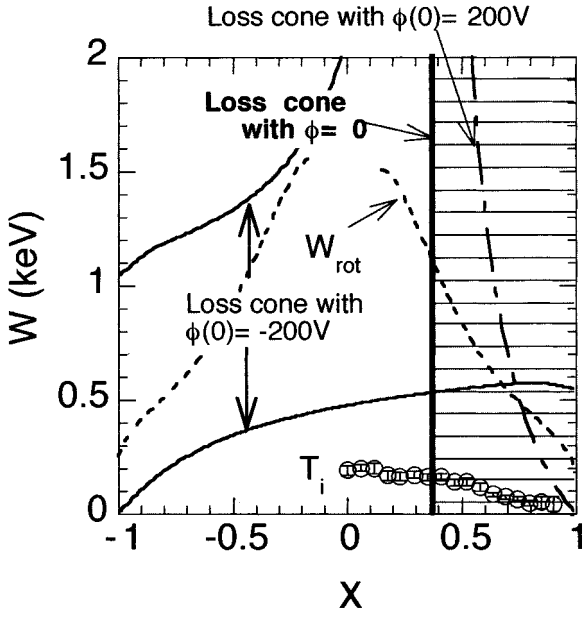

FIG. 5. Comparison between loss cone structures with and without potential. The loss cone without potential is located at of $\rho > 0.37$ on the low field side of plasma, and is independent of the particle energy. Note that the particle energy is shown in a linear scale. For comparison, the loss cone boundary for a potential with the same magnitude but opposite sign from the measured potential is indicated by the dot–dashed line.

positive potential the ion loss cone region is localized to the outside periphery of the plasma. The loss cone boundary is shown by the dashed line in Fig. 4(b). The dashed line in Fig. 4(a) shows the loss cone for deeply trapped electrons in the NBI plasma.

In order to demonstrate the effect of potential on the loss cone structure, Fig. 5 shows the loss cone for deeply trapped ions without potential ($\phi \equiv 0$) on a linear scale, together with the loss cone in the NBI plasma. The loss cone without potential covers locations with $\rho > 0.37$ on the weak field side and is not dependent on particle energy. As a result, the bulk ion temperature is in this loss cone region, although the energy may be lower than $W_{\rm rot}$. For comparison, the loss cone boundary indicated by the dashed line is for a potential profile with the same absolute value as the measured profile, but with the opposite sign; $\phi(0) = 200$ V. The potential profile is self-consistently determined by a balance between electron and ion fluxes, including the loss cone loss. The measured bulk ion temperature is located below the wider loss cone region, which is caused by the helical resonance.

The present loss cone analysis suggests that a high heating efficiency and confinement of high-energy particles can be realized if a positive potential profile can be kept in a NBI-heated plasma with an effective use of ECH. The heating efficiencies for electrons and ions in toroidal helical plasmas can be ameliorated or deteriorated for different electrostatic potentials. Actually, in the Wendelstein VII-A (WVII-A) experiments a high confinement condition was attained in discharges with perpendicular NBI heating when a strong negative potential was created.[17] In addition, the recent discovery of a high ion temperature mode in the Heliotron-E plasma may be related to the strong electric field shear.[18]

V. DISCUSSION AND SUMMARY

The complete radial potential profile measurements presented here made it possible to find the fine spatial structure of the electric field profile. In the medium-density ECH plasma, the electric field changes from positive in the center

to negative at the edge. For this case, an exhaustive numerical calculation would be necessary to evaluate the loss cones. The strong shear of the electric field around the edge gives a hint of turbulence suppression. A theory based on stabilization of interchange instabilities suggests that the strong shear may result in suppression of fluctuation-driven transport by a few percents.[19] At the level of plasma heating (~ 100 kW) in this experiment, the turbulence suppression is expected to be marginal.

Efforts have been made on CHS to evaluate the radial electric field with the CXS measurements.[9,10] The deduced electric field profile in a NBI-heated plasma similar to the one presented here ($\overline{n_e}=6.5\times10^{12}$ cm^{-3}) indicated $E_r=0 \pm 10$ V/cm. The error bar arises from the fact that the number of photons was limited for that density regime. On the other hand, the HIBP shows that the electric field of the NBI plasma is clearly negative.

The momentum balance equation $\nabla P_\alpha = eZ_\alpha n_\alpha(\mathbf{E}+\mathbf{v}_\alpha\times\mathbf{B})+\mathbf{R}_\alpha$ is used to evaluate the radial electric field from impurity rotation velocity measurements with an assumption that the friction force $\mathbf{R}_\alpha=0$. Here, P_α, Z_α, n_α, and v_α are the pressure, the charge, the density, and the velocity of the impurity identified by α, respectively. Presently, in higher electron density regimes ($n_e>2\times10^{13}$ cm^{-3}), strong uv radiation from the plasma affects the power supplies of the HIBP secondary beam sweep system. This problem will be solved easily by increasing the power supply current capacity in the near future. Then, simultaneous measurements of the electric field profiles (HIBP) and impurity velocities (CXS) will allow an estimate of this friction force acting on impurities, and give new insight into impurity transport.

In summary, we have directly measured internal potential profiles in a toroidal helical plasma of the CHS heliotron/torsatron, using a HIBP with a newly proposed beam control method. The potential profiles show a clear difference in ECH and NBI plasmas that exhibit electron (positive electric field) and ion root (negative electric field) characteristics, respectively. Confinement properties and heating efficiency of a low aspect ratio toroidal helical plasma can be improved by controlling the loss cone structure through the potential profile. Therefore, direct measurements of potential are essential to clarify the physical mechanism of potential formation, which will be a key issue when searching for better confinement regimes in toroidal helical plasmas.

ACKNOWLEDGMENTS

The authors are very grateful to Dr. M. Fujiwara for his continuous encouragement. The authors also acknowledge useful discussions with Dr. S-I. Itoh. Acknowledgements are given to the CHS experimental group.

[1] B. B. Kadomtsev and O. P. Pogutse, Nucl. Fusion **11**, 67 (1971).
[2] B. A. Carreras, N. Dominguez, L. Garcia, V. E. Lynch, J. F. Lyon, J. R. Cary, J. D. Hanson, and A. P. Navarro, Nucl. Fusion **28**, 1195 (1988).
[3] The ASDEX Team, Nucl. Fusion **29**, 1959 (1989).
[4] K. Itoh and S-I. Itoh, Phys. Controlled Fusion **38**, 1 (1996).
[5] G. A. Hallock, J. Mathew, W. C. Jennings, R. L. Hickok, A. J. Wootton, and R. C. Isler, Phys. Rev. Lett. **56**, 1248 (1986).
[6] X. Z. Yang, B. Z. Zhang, A. J. Wootton, P. M. Schoch, B. Richards, D. Baldwin, D. L. Brower, G. G. Castle, R. D. Hazeltine, J. W. Heard, R. L. Hickok, W. L. Li, H. Lin, S. C. McCool, V. J. Simcic, Ch. P. Ritz, and C. X. Yu, Phys. Fluids B **3**, 3448 (1991).
[7] S. C. Aceto, K. A. Connor, J. G. Schwelberger, and J. J. Zielinski, IEEE Trans. Plasma Sci. **PS-22**, 388 (1994).
[8] K. Matsuoka, S. Kubo, M. Hosokawa, Y. Takita, S. Okamura, N. Node, H. Yamada, H. Iguchi, K. Masai, S. Morita, K. Ida, H. Idei, C. Takahashi, K. Nishimura, T. Shoji, H. Sanuki, M. Fujiwara, Y. Abe, T. Amano, A. Ando, T. Aoki, D.-G. Bi, J. Fujita, S. Hidekuma, T. Kamimura, O. Kaneko, T. Kawamoto, A. Mohri, A. Nishizawa, S. Tanahashi, J. Todoroki, K. Tsuzuki, and K. Yamazaki, in *Plasma Physics and Controlled Nuclear Fusion Research 1988*, Proceedings of the 12th International Conference, Nice, 1988 (International Atomic Energy Agency, Vienna, 1989), Vol. 2, p. 411.
[9] K. Ida, H. Yamada, H. Iguchi, S. Hidekuma, H. Sanuki, and K. Yamazaki, Phys. Fluids B **3**, 515 (1991).
[10] H. Idei, K. Ida, H. Sanuki, H. Yamada, H. Iguchi, S. Kubo, R. Akiyama, H. Arimoto, M. Fujiwara, M. Hosokawa, K. Matsuoka, S. Morita, K. Nishimura, K. Ohkubo, S. Okamura, S. Sakakibara, C. Takahashi, Y. Takita, K. Tsumori, and I. Yamada, Phys. Rev. Lett. **71**, 2220 (1993).
[11] A. Fujisawa, H. Iguchi, M. Sasao, Y. Hamada, and J. Fujita, Rev. Sci. Instrum. **63**, 3694 (1992).
[12] A. Fujisawa, H. Iguchi, S. Lee, T. P. Crowley, Y. Hamada, S. Hidekuma, and M. Kojima, Rev. Sci. Instrum. **67**, 3099 (1996).
[13] H. Sanuki, K. Itoh, and S-I. Itoh, J. Phys. Soc. Jpn. **62**, 123 (1993).
[14] D. E. Hastings, W. A. Houlberg, and K. C. Shaing, Nucl. Fusion **25**, 445 (1985).
[15] L. M. Kovrizhnykh, Nucl. Fusion **24**, 435 (1984).
[16] K. Itoh, S-I. Itoh, A. Fukuyama, and K. Hanatani, Nucl. Fusion **29**, 1851 (1989).
[17] H. Wobig, H. Maassberg, H. Renner, The WVII-A Team, the ECRH Group, and the NI Group, in *Plasma Physics and Controlled Nuclear Fusion Research*, Proceedings of the 11th International Conference, Kyoto, 1986 (International Atomic Energy Agency, Vienna, 1987), Vol. 2, p. 369.
[18] K. Ida, K. Kondo, K. Nagasaki, T. Hamada, S. Hidekuma, F. Sano, H. Zushi, T. Mizuuchi, H. Okada, S. Besshou, H. Funaba, K. Watanabe, and T. Obiki, Phys. Rev. Lett. **76**, 1268 (1996).
[19] K. Itoh, S-I. Itoh, A. Fukuyama, H. Sanuki, and M. Yagi, Plasma Phys. Controlled Fusion **36**, 123 (1994).